PCCP

ROYAL SOCIETY OF CHEMISTRY

PAPER

View Article Online
View Journal | View Issue

Cite this: *Phys. Chem. Chem. Phys.*, 2022, **24**, 20546

Pressure-induced phase transition in α- and β-$BiNbO_4$†

HPSTAR 1515-2022

Xingbang Dong,[ab] Zhanbiao Huangfu,[ab] Shiquan Feng,[ab] Yongfu Liang,[ab] Huanjun Zhang,[ab] Xiang Zhu,[ab] Kun Yang,[ab] Zheng Wang,*[ab] Xuerui Cheng*[ab] and Lei Su*[cd]

Received 5th July 2022,
Accepted 26th July 2022

DOI: 10.1039/d2cp03040c

rsc.li/pccp

$BiNbO_4$ has attracted a great deal of interest due to its excellent photocatalytic activities. Besides, it possesses rich polymorphism. Here, the structural stability and structural evolution of orthorhombic α- and triclinic β-$BiNbO_4$ were investigated *via in situ* X-ray diffraction patterns and Raman spectra up to 46.7 GPa. Upon compression, both $BiNbO_4$ samples become unstable. α-$BiNbO_4$ transformed into the *monoclinic C2/c* structure at 10.3 GPa, while β-$BiNbO_4$ possessed one $P\bar{1}$-to-*P*1 isostructural phase transition around 12.7 GPa, and for the first time the crystal structure of each high pressure phase was identified. Both high pressure structures remained stable without obvious symmetry changes during compression to 46.7 GPa. In addition, both phase transitions were reversible upon decompression. These results provide insights to understand pressure-induced reversible phase transition in ABO_4 compounds with polymorphism.

Introduction

Recently, bismuth-based photocatalysts have attracted great interest due to their rich crystal chemistry, diverse chemical compositions and adjustable electronic band structure for a visible light response.[1–4] Among them, $BiNbO_4$ is one of the most promising compounds because of its unique band structure and good photocatalytic performance.[5–9] In addition, $BiNbO_4$ possesses rich polymorphism and four polymorphs have been reported, namely, the orthorhombic α-$BiNbO_4$ with a space group of *Pnna*,[10] triclinic β-$BiNbO_4$ with a space group of $P\bar{1}$,[11] orthorhombic γ-$BiNbO_4$ with a space group of $Cmc2_1$ and cubic HP-$BiNbO_4$ with a space group of $Fd\bar{3}m$.[12,13] All these $BiNbO_4$ polymorphs are built by BiO_6 and NbO_6 octahedra but with different arrangements, resulting in quite different physical properties. For example, α-$BiNbO_4$ exhibits better photocatalytic activity while β-$BiNbO_4$ shows potential for application in photoluminescence and scintillation.[14] Because of its rich polymorphism and excellent physical properties, structural stability and structural evolution in $BiNbO_4$ is an interesting topic and has been extensively investigated.[15]

Using the solid state reaction, α-$BiNbO_4$ can be synthesized through Bi_2O_3 and Nb_2O_5 at 900 °C while β-$BiNbO_4$ can be obtained above 1150 °C.[8] This result has been attributed to the α-to-β irreversible transition at 1020 °C for $BiNbO_4$. In contrast, Zhuk *et al.* observed that α-$BiNbO_4$ transformed into another new high temperature phase, γ-$BiNbO_4$ rather than β-$BiNbO_4$ after annealing α-$BiNbO_4$ above 1055 °C.[12,16] Moreover, the high temperature phase γ-$BiNbO_4$ is unstable and it can convert back to β-$BiNbO_4$ in the cooling process below 997 °C. Besides, the above transition is reversible that β-$BiNbO_4$ will transform into γ-$BiNbO_4$ above 1001 °C again with a normal heating process. Therefore, this suggests that the previously reported α-to-β irreversible transition during the heating–cooling process is actually the α → γ → β transition. Moreover, it has been believed that α-$BiNbO_4$ could not be obtained from β-$BiNbO_4$ because of the above α → γ → β transition. However, recently, an abnormal β-to-α transition has been observed above 950 °C at a slow heating process for $BiNbO_4$.[17–19] Besides temperature, doping can also induce phase transition between different $BiNbO_4$ polymorphs. It has been reported that β-$BiNbO_4$ turns unstable upon doping and it would gradually transform into α-$BiNbO_4$ with the increase of the Eu^{3+} doping concentration.[20] And doping can also change the α-to-β transition temperature, such as copper, manganese or nickel doping.[21–24] Zhuk *et al.* reported that α-to-β transition temperature could increase on average by 100 °C with the increase of the copper oxide content.[21] In addition, pH of a precursor also has a great effect on the phase stability of $BiNbO_4$. In the co-precipitation

[a] *School of Physics and Electronic Engineering, Zhengzhou University of Light Industry, Zhengzhou, Henan, 450002, China. E-mail: wz7907@163.com, xrcheng@zzuli.edu.cn*
[b] *Henan key laboratory of magnetoelectric information functional materials, Zhengzhou, Henan, 450002, China*
[c] *Center for High Pressure Science and Technology Advanced Research, 100094 Beijing, China. E-mail: lei.su@hpstar.ac.cn*
[d] *Key Laboratory of Photochemistry, Institute of Chemistry, University of Chinese Academy of Sciences, Chinese Academy of Sciences, Beijing, 100190, China*
† Electronic supplementary information (ESI) available. See DOI: https://doi.org/10.1039/d2cp03040c

method, a high pH will result in the β-$BiNbO_4$ structure while low pH promotes the formation of α-$BiNbO_4$.[25]

Besides temperature, doping and pH, pressure is also extensively investigated as another approach to discover and access new structures or novel properties of materials. It has been reported that a new metastable phase of $BiNbO_4$, HP-$BiNbO_4$, could be obtained from α-$BiNbO_4$ or β-$BiNbO_4$ at 5 GPa and 800 °C.[13] This HP-$BiNbO_4$ is stable during further compression and no pressure-induced phase transition has been observed up to 24.1 GPa.[26] However, this metastable HP-$BiNbO_4$ phase will convert back to α-$BiNbO_4$ and β-$BiNbO_4$ again after heating above 600 °C and 1150 °C, respectively. Furthermore, α-$BiNbO_4$ is also unstable under pure high-pressure conditions, and experiences a reversible phase transition at 10.3 GPa at room temperature.[27] However, the detailed structural information of this new HP-phase is still unclear. Moreover, to the best of our knowledge, there have been no studies on the structural stability of other two metastable structures (β- and γ-$BiNbO_4$) under pressure. Therefore, despite much effort made in the past, a full understanding of the structural evolution of $BiNbO_4$ under pressure was not yet achieved and additional research is required to extend previous studies for $BiNbO_4$.

In view of the above aims, α-$BiNbO_4$ and β-$BiNbO_4$ were successfully synthesized and the effect of pressure on both structural stability and phase behavior was investigated using *in situ* X-ray diffraction patterns and Raman spectra up to 46.7 GPa. Moreover, the effect of hydrostatic pressure conditions on the structural evolution has been investigated by using two different pressure transmitting media (silicon oil and Ar gas). These results will be helpful for a more in-depth understanding of the phase transition in $BiNbO_4$.

Experiment

Two types of $BiNbO_4$ samples were synthesized using the solid state method. The starting materials are Nb_2O_5 and Bi_2O_3 with purity of 99.9%. Both starting materials were weighted according to a stoichiometric ratio (Bi : Nb = 1 : 1) and then efficiently ground *via* a mortar and pestle. The obtained precursor was firstly pre-heated at 700 °C for 48 h in a muffle furnace to avoid the volatility of the Bi element. Then, it was cracked and ground again. Part of the powder was calcined at 900 °C for 48 h and the rest was calcined at 1200 °C for 24 h. After heat treatment, the obtained samples were ground again for the following characterization.

The crystal structure and phase purity were characterized by X-ray diffraction, excited with Cu Kα radiation (Ultima IV, Rigaku, 1.540598 Å, 40 kV, 40 mA). The Raman spectrum was measured using a Renishaw inVia Raman microscope (Renishaw, UnitedKingdom) with a 532 nm laser. Raman spectra were collected in backscattering geometry using a 2400 g mm^{-1} grating and the slit width was selected as 65 μm with a resolution of *ca.* 0.5 cm^{-1}. All the measurements were conducted at room temperature.

The high pressure experiments were performed using a diamond anvil cell (DAC) with a diamond culet of 300 μm. The $BiNbO_4$ samples and ruby were loaded into a hole with a diameter of 170 μm and a thickness of 50 μm (pre-indented) in a steel gasket. The pressure was determined *via* the shift of the ruby R_1 emission line.[28] To maintain hydrostatic conditions around samples, argon gas serves as the pressure transmitting medium (PTM).[29] The high-pressure (HP) Raman measurements were *in situ* performed using a Renishaw inVia Raman microscope spectrometer. The Raman acquisition parameters are set consistent with the above atmospheric pressure measurements. The pressure was applied at a step of about 1 GPa, and the Raman spectra were collected at each pressure point. Then, the selected Raman spectrum was processed and further analysed. The HP-XRD experiments were performed at the BL15U1 beamline of Shanghai Synchrotron Radiation Facility. The 2D diffraction images were collected with a Mar CCD detector using monochromatic radiation with a wavelength of 0.6199 Å. High-purity CeO_2 powder was used to calibrate the geometrical parameters of the detector. The images were transformed into patterns of intensity *versus* 2θ using DIOPTAS.[30]

The theroretical calculations of this work are carried out using the Vienna *Ab initio* Simulation Package (VASP) based on density functional theory. The generalized gradient approximation (GGA) was chosen as the exchange–correlation potential function.[31,32] The plane-wave cutoff energy is set as 520 eV. The Monkhorst–Pack scheme was adopted to set k points in the Brillouin zone. And the k point meshes were adopted as $6 \times 3 \times 7$ and $4 \times 6 \times 4$ for α-$BiNbO_4$ and β-$BiNbO_4$, respectively. For structural optimization at high pressures, the systems were relaxed until the total energy and ionic Hellmann–Feynman force became less than 1×10^{-6} eV per atom and 0.02 eV $Å^{-1}$, respectively. In the calculation process, the Bi $6s^26p^3$, Nb $4d^45s^1$ and O $2s^22p^4$ electrons were treated as valence states.

Results and discussion

The crystal structures of α-$BiNbO_4$ and β-$BiNbO_4$ are shown in Fig. 1. α-$BiNbO_4$ has a one layer structure, composed of bismuth layers and NbO_6 octahedral layers. The NbO_6 octahedron in each layer is connected to each other by corner-sharing of oxygen atoms. And the Bi^{3+} cations isolated each NbO_6 octahedral layer in a straight line arrangement along the *b* axis, as shown in Fig. 1(a). β-$BiNbO_4$ exhibits a similar crystal structure arrangement to that of α-$BiNbO_4$ while its NbO_6 octahedral layers are wrinkled, as shown in Fig. 1(b), resulting in more-efficient stacking and relatively larger density than the α-phase. Moreover, for both Bi^{3+} and Nb^{5+} ions, each element occupies one kind of crystal sites in α-$BiNbO_4$, while there are two different sites for each kind of Bi^{3+} or Nb^{5+} ions in β-$BiNbO_4$. Therefore, the crystal symmetry of β-$BiNbO_4$ is much lower than that of α-$BiNbO_4$.

Fig. 2(a) presents the XRD patterns of $BiNbO_4$ samples calcined at 900 °C and 1200 °C, respectively. The sharp and well-defined diffraction peaks suggest the good crystallinity of

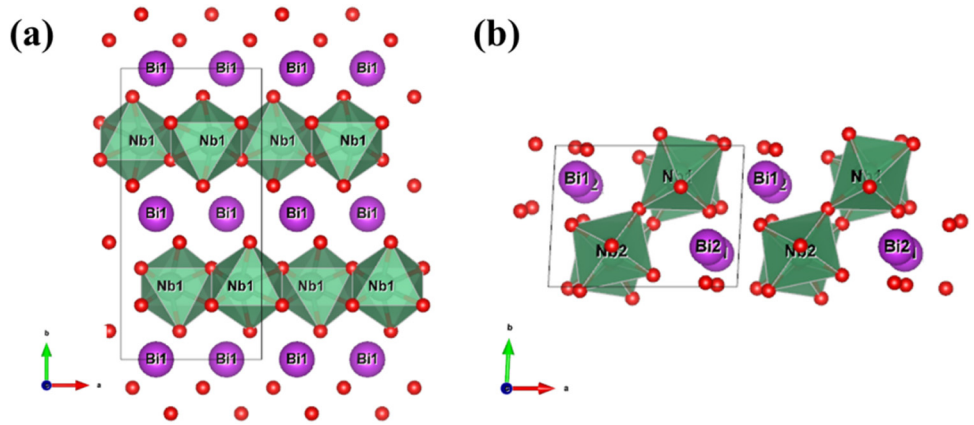

Fig. 1 Crystal structures of (a) α- and (b) β-$BiNbO_4$ (the Bi, Nb and O atoms are denoted in purple, green and red colors, respectively. The unit cell is shown in a dashed line).

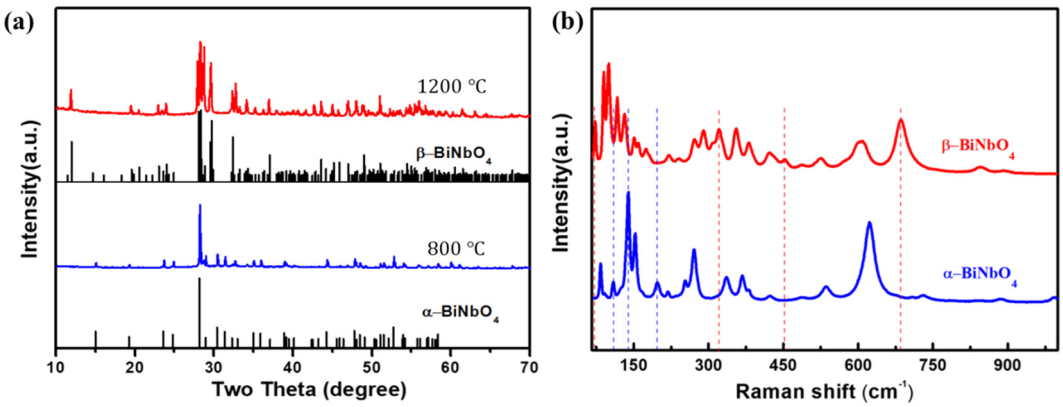

Fig. 2 The (a) XRD patterns and (b) Raman spectra of α- and β-$BiNbO_4$. The dotted line highlights their structural difference in the Raman spectrum.

two $BiNbO_4$ samples. The diffraction peaks of both $BiNbO_4$ samples can be well indexed to those of α-$BiNbO_4$ (orthorhombic, ICSD:74338) and β-$BiNbO_4$ (triclinic, ICSD:10247), respectively. No other diffraction peaks of the impurity phase can be detected. Therefore, the XRD results indicate that two $BiNbO_4$ samples were successfully synthesized. Fig. 2(b) shows the Raman spectrum of two $BiNbO_4$ samples. The Raman results match well with those of previous report,[33] further suggesting the successful synthesis of α- and β-$BiNbO_4$. For α-$BiNbO_4$, the vibrational modes at 624 cm^{-1} and 534 cm^{-1} correspond to A_{1g} and E_g, originating from the internal stretching vibration mode of the NbO_6 octahedron.[34] The peaks at 271 cm^{-1} and 197 cm^{-1} are ascribed to two angular bending vibrational modes of F_{2g} and F_{2u}, respectively.[35] The peaks located at 367 cm^{-1}, 383 cm^{-1} and 425 cm^{-1} are assigned to F_{1u} modes. The peak at 886 cm^{-1} can be attributed to the stretching vibration of the octahedron of BiO_6. As shown in Fig. 2, the XRD patterns and Raman spectra of β-$BiNbO_4$ are much more complicated than those of α-$BiNbO_4$, which may be attributed to the lower symmetry and more complex structural arrangement of β-$BiNbO_4$, as discussed above.

The structural stability and phase behavior of α- and β-$BiNbO_4$ under high pressure were investigated *via* the *in situ* Raman spectra up to 39.7 GPa and 38.1 GPa, respectively. The Ar gas was used as the PTM to ensure the hydrostatic pressure condition. As shown in Fig. 3(a), α-$BiNbO_4$ remains stable below 4.9 GPa while several new Raman bands appear at around 188, 283, 330, 758 and 857 cm^{-1} above this pressure. When the pressure is increased up to 10.3 GPa, more new Raman peaks are observed at 143, 182, 368, 454, 553, 677 and 719 cm^{-1}, respectively. Upon further increasing the pressure, the intensity of these new peaks becomes gradually strengthened. Meanwhile, the intensity of original Raman modes of α-$BiNbO_4$ evidently weakens, especially for its dominant mode at 639 cm^{-1}. These variations suggest one pressure-induced phase transition at 10.3 GPa for α-$BiNbO_4$, which matches well with the previously reported XRD results.[27] Upon further compression, no distinct changes are detected except that most of the Raman modes become weak and broad. Up to the maximum pressure of 39.1 GPa, only a prominent broad band at 778 cm^{-1} and several weaken modes below 300 cm^{-1} can be detected.

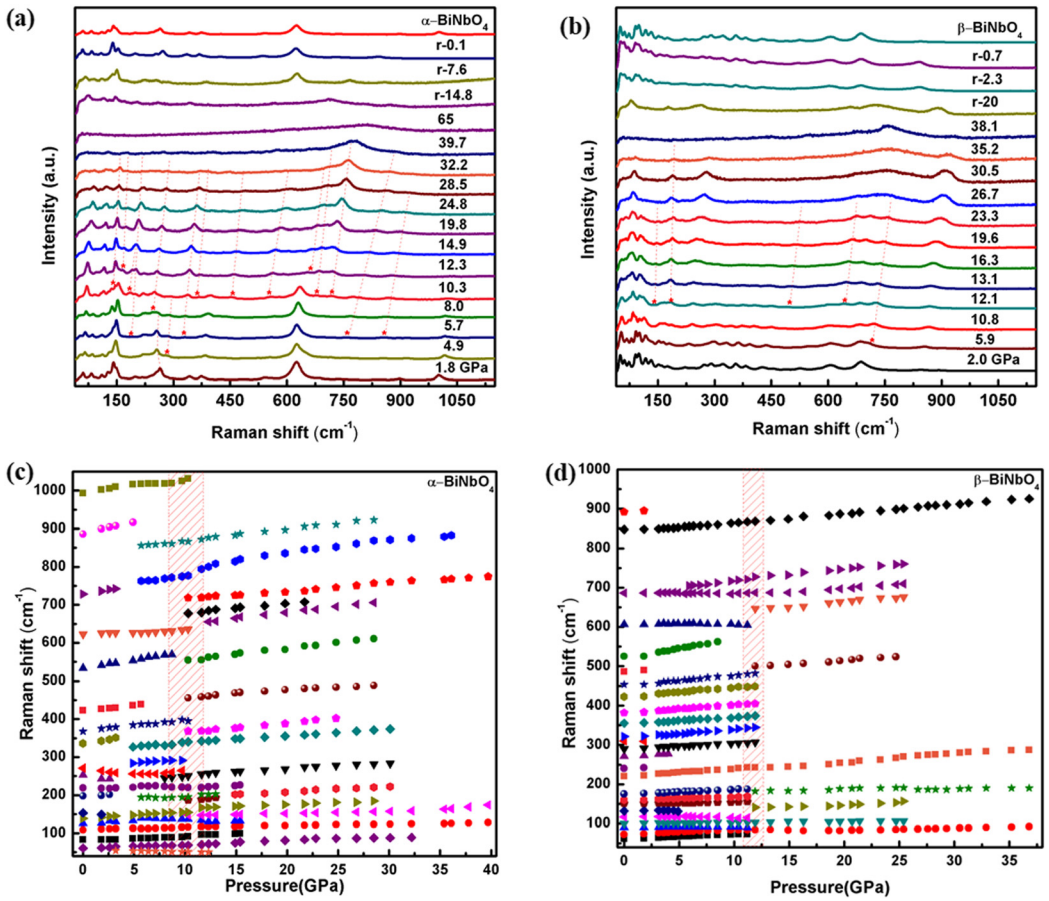

Fig. 3 The evolution of Raman spectra under pressure of (a) α- and (b) β-$BiNbO_4$. Frequency shift of Raman modes as a function of pressure of (c) α- and (d) β-$BiNbO_4$.

Similar results are also observed for β-$BiNbO_4$, as shown in Fig. 3(b). No distinct changes are detected in the Raman patterns below 12.1 GPa. Then, several new Raman modes appear at 137, 182, 497 and 647 cm^{-1} at 12.1 GPa and become more prominent at higher pressure. Simultaneously, several sharp Raman peaks in the low frequency region gradually merge or disappear. These changes mean that there is one structural transformation for β-$BiNbO_4$ at 12.1 GPa as well. Similar to that of α-$BiNbO_4$, upon further compression, most of the Raman peaks become weak and broad, and only a prominent broad band at 758 cm^{-1} can be clearly observed up to the maximum pressure of 38.1 GPa.

The pressure-induced variations in the Raman spectrum of α- and β-$BiNbO_4$ can be clearly observed in Fig. 3(c) and (d). Evidently, most Raman modes shift toward the higher frequencies during compression. Obvious discontinuity can be observed at about 10.3 and 12.1 GPa for α-$BiNbO_4$ and β-$BiNbO_4$, respectively. These variations clearly suggest one phase transition for each sample in the current pressure region. In addition, after decompression to the ambient pressure, the Raman spectra of two high pressure phases convert back to the original spectra of α- and β-$BiNbO_4$, indicating that both phase transitions are completely reversible for α- and β-$BiNbO_4$.

It is well known that the choice of PTM has a great influence on the surrounding hydrostatic conditions and thus affects the high pressure behavior of compounds.[36] To further confirm the pressure-induced phase transition of both $BiNbO_4$ samples and eliminate the influence of the PTM, high-pressure experiments were performed again for both samples using silicon oil as the PTM. From Fig. S1 (ESI†), it can be found that the evolutions of Raman spectra under pressure are similar to that using Ar gas as the PTM. Even the transition pressures are similar for two different PTMs. Therefore, it can be confirmed that there exists a pressure-induced phase transition around 10.3 and 12.1 GPa, respectively, in α- and β-$BiNbO_4$, no matter of PTM.

To further confirm the structural evolution of two types of $BiNbO_4$, HP-XRD measurements were performed. Fig. 4 shows the evolution of XRD patterns for both $BiNbO_4$ structures in the compression and decompression process. As shown in Fig. 4, with increasing pressure, all diffraction peaks move towards higher diffraction angles due to the pressure-induced contraction of d-spacing. Upon increasing the pressure to 10.1 GPa, three new diffraction peaks appear at 6.8°, 11.7° and 13.8° for α-$BiNbO_4$, and these new peaks gradually become dominant with increasing pressure. Meanwhile, the original diffraction peaks at 6°, 10° and 12.5° gradually disappear above 13.0 GPa. Upon further increasing the pressure, no distinct changes are

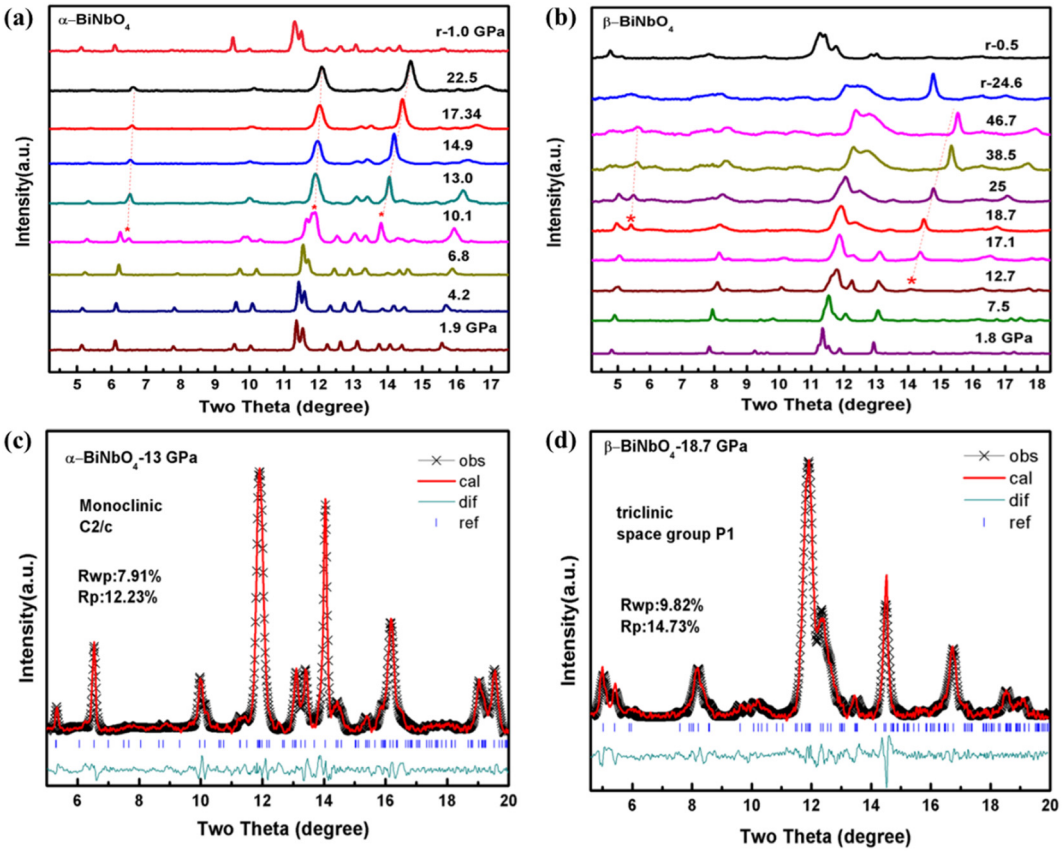

Fig. 4 Selected X-ray diffraction patterns of (a) α- and (b) β-$BiNbO_4$ under pressure. The red asterisk denotes the presence of new diffraction peaks. Rietveld refinement of the high pressure phase of (c) α- and (d) β-$BiNbO_4$ at specific pressure.

detected except that most of the diffraction peaks become weak and broad. For β-$BiNbO_4$, a new diffraction peak is observed around 14.1° at 12.7 GPa, and then another new diffraction peak appears at 5.4° at 18.7 GPa. Upon continuous compression, the diffraction peak at 11.9° becomes dominant above 25 GPa, but no other changes are observed. The evolution of XRD patterns matches well with the changes observed in the above Raman spectra, further confirming the pressure-induced phase transition for α- and β-$BiNbO_4$ around 10.3 and 12.1 GPa. Moreover, compared with the results of phonon dispersion for α- and β-$BiNbO_4$ at ambient pressure,[37] imaginary frequencies are observed for both structures under a high pressure of 13 GPa, as shown in Fig S2 (ESI†). This confirms that both phases become unstable at high pressure, which indirectly proves that they have experienced phase transition. During decompression, the XRD spectra of both high-pressure phases can convert back to the initial spectra of α and β structures. But for β-$BiNbO_4$, it is interesting to note that the Raman spectra recovered from 38.1 GPa are almost the same as those of the initial β structure. While its XRD peaks recovered from 46.7 GPa are more broader than those of the initial structure. This difference may be attributed to the crystal structure distortion upon higher pressure.

Structural refinement was performed for each high pressure phase of α- and β-$BiNbO_4$ to identify the crystal structure. The fitting results are shown in Fig. 4(c) and (d). The diffraction pattern of the high-pressure phase of α-$BiNbO_4$ at 13 GPa matches well with that of *monoclinic* structure $BiNbO_4$ with a space group of *C*2/*c*. The *R*-factors of this refinement are R_{wp} = 7.91% and R_p = 12.23%. While the high-pressure phase of β-$BiNbO_4$ at 18.7 GPa can be indexed to the triclinic $BiNbO_4$ with a space group of *P*1. Its *R*-factors obtained are R_{wp} = 9.82% and R_p = 14.73%. Therefore, it can be confirmed that α-$BiNbO_4$ experiences one reversible *Pnna*-to-*C*2/*c* transition at 10.1 GPa, while β-$BiNbO_4$ possesses one reversible $P\bar{1}$-to-*P*1 isostructural phase transition at 12.1 GPa. And this is for the first time the high-pressure structure of α-$BiNbO_4$ is identified, and for the first time the pressure-induced phase transition for β-$BiNbO_4$ is reported. It has been reported that either α-$BiNbO_4$ or β-$BiNbO_4$ will transform into cubic HP-$BiNbO_4$ at 5 GPa and 800 °C. But here, this cubic phase has not been observed under pure pressure conditions for both samples. This result suggests that high temperature is one necessary thermodynamic parameter to obtain cubic HP-$BiNbO_4$.

In our previous research on ABO_4 compounds, such as $BiVO_4$,[38,39] $ZrGeO_4$[40] and $LaVO_4$,[41] it is believed that different polymorphic compounds will finally transform into the same high-pressure structure if the pressure is high enough. For example, the fergusonite- and zircon-type $BiVO_4$ finally transform into the same scheelite-$BiVO_4$ at high pressure. The

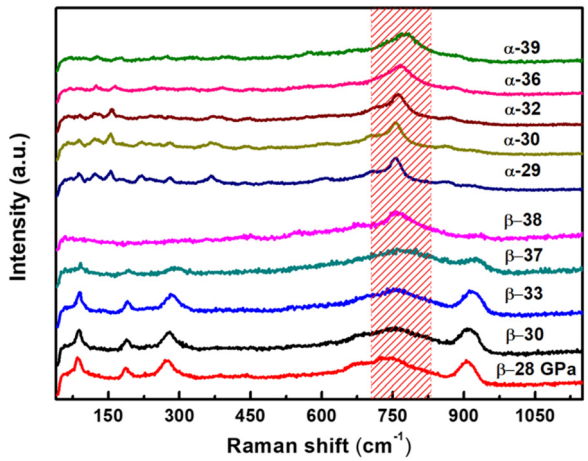

Fig. 5 Comparison of the Raman results of α- and β-$BiNbO_4$.

similar results have also been observed in $ZrGeO_4$ and $LaVO_4$. Thus, it is reasonable to speculate that α- and β-$BiNbO_4$ are likely to be converted to the same high-pressure structure under sufficient compression. As compared in Fig. 5, most of the Raman peaks of two β-$BiNbO_4$ samples become weak upon compression and finally only one main broad peak around 759 cm^{-1} can be observed. At above 38.5 GPa, both samples have similar Raman spectra. Thus, it is highly likely that both samples tend to exhibit the same Raman spectra and convert into the same high pressure structure at higher pressure. However, this speculation has not been verified here because of the limited pressure used in present work.

Conclusion

Orthorhombic α- and triclinic β-$BiNbO_4$ compounds were successfully synthesized using the solid state method. The structural stability of both $BiNbO_4$ samples under pressure was investigated *via* the *in situ* Raman spectrum and XRD patterns. The results show a reversible phase transition for α-$BiNbO_4$ at 10.3 GPa, from *Pnna*-to-*C*2/*c* and that for β-$BiNbO_4$ at 12.7 GPa, from $P\bar{1}$-to-*P*1. The high pressure phase of both $BiNbO_4$ samples was identified for the first time from structural refinement. The same high pressure phase was not observed for both types of $BiNbO_4$ in this study due to the insufficient compression. Moreover, both phases show the same phase transition pressure and sequence under different PTMs (silicon oil and Ar gas). This confirms the pressure-induced phase transition in both $BiNbO_4$ samples. The high-pressure behavior of $BiNbO_4$ is different from our previous research, which provides another perspective of the pressure behavior of AVO_4 compounds with polymorphism.

Conflicts of interest

The authors declare no conflict of interest.

Acknowledgements

This work was supported by the National Science Foundation of China (No. 12104415), Key Research Project of Department of Science and Technology in Henan Province (No. 222102230012 and No. 222102210180), and Key Research Project of Higher Education of Henan Province (No. 21B140011 and 22B430031). We also thank Dr Chaosheng Yuan for providing Raman spectrograph.

References

1 S. Wang, L. Wang and W. Huang, Bismuth-based photocatalysts for solar energy conversion, *J. Mater. Chem. A*, 2020, **8**, 24307–24352.
2 L. Zhang, Y. Li, Q. Li, J. Fan, S. A. C. Carabineiro and K. Lv, Recent advances on Bismuth-based Photocatalysts: Strategies and mechanisms, *Chem. Eng. J.*, 2021, **419**, 129484.
3 J. H. Kim and J. S. Lee, Elaborately Modified $BiVO_4$ Photoanodes for Solar Water Splitting, *Adv. Mater.*, 2019, **31**, 1806938.
4 E. Aksel, P. Jakes, E. Erdem, D. M. Smyth, A. Ozarowski, J. van Tol, J. L. Jones and R. A. Eichel, Processing of Manganese-Doped Bi0.5Na0.5TiO3 Ferroelectrics: Reduction and Oxidation Reactions During Calcination and Sintering, *J. Am. Ceram. Soc.*, 2011, **94**, 1363–1367.
5 M. Kuznetsova, S. A. A. Oliveira, B. S. Rodrigues and J. S. Souza, Microwave-Assisted Synthesis of Bismuth Niobate/Tungsten Oxide Photoanodes for Water Splitting, *Top. Catal.*, 2021, **64**, 748–757.
6 J. Nisar, B. C. Wang, B. Pathak, T. W. Kang and R. Ahuja, Mo- and N-doped $BiNbO_4$ for photocatalysis applications, *Appl. Phys. Lett.*, 2011, **99**, 051909.
7 S. Xiong, Y. Liu, T. Li, F. Li and W. Cao, A facile hydrothermal preparation of O-deficient $BiNbO_4$ nanorods for effective sonocatalytic decontamination, *Ceram. Int.*, 2020, **46**, 21790–21793.
8 S. S. Dunkle and K. S. Suslick, Photodegradation of $BiNbO_4$ Powder during Photocatalytic Reactions, *J. Phys. Chem. C*, 2009, **113**, 10341–10345.
9 W. Jo, E. Erdem, R. A. Eichel, J. Glaum, T. Granzow, D. Damjanovic and J. Roedel, Effect of Nb-donor and Fe-acceptor dopants in (Bi1/2Na1/2)TiO3-BaTiO3-(K0.5Na0.5)NbO3 lead-free piezoceramics, *J. Appl. Phys.*, 2010, **108**, 014110.
10 M. A. Subramanian and J. C. Calabrese, Crystal structure of the low temperature form of bismuth niobium oxide α-$BiNbO_4$, *Mater. Res. Bull.*, 1993, **28**, 523–529.
11 E. T. Keve and A. C. Skapski, The crystal structure of triclinic β-$BiNbO_4$, *J. Solid State Chem.*, 1973, **8**, 159–165.
12 N. A. Zhuk, M. G. Krzhizhanovskaya, V. A. Belyy and B. A. Makeev, High-Temperature Crystal Chemistry of α-, β-, and γ-$BiNbO_4$ Polymorphs, *Inorg. Chem.*, 2019, **58**, 1518–1526.
13 C. Xu, D. He, C. Liu, H. Wang, L. Zhang, P. Wang and S. Yin, High pressure and high temperature study the phase

transitions of $BiNbO_4$, *Solid State Commun.*, 2013, **156**, 21–24.
14 R. Yu, A. Fan, M. Yuan, T. Li and J. Wang, Observation of intrinsic emission in β-$BiNbO_4$ available for excitation of both UV light and high energy irradiation, *Phys. Chem. Chem. Phys.*, 2016, **18**, 23702–23708.
15 C. Yu, G. Viola, D. Zhang, Z. Stroscio, Z. Hu, V. R. Eskilla, S. Grasso, R. M. Wilson, K. Zhou, N. Bonini, A. D. Fortes, I. Abrahams and H. Yan, Structural Evolution in $BiNbO_4$, *Inorg. Chem.*, 2021, **60**, 8507–8518.
16 N. A. Zhuk, B. A. Makeev, V. A. Belyy and M. G. Krzhizhanovskaya, Thermal analysis and high-temperature X-ray diffraction study of $BiNbO_4$, *J. Therm. Anal. Calorim.*, 2019, **137**, 1513–1518.
17 H.-F. Zhai, X. Qian, J.-Z. Kong, A.-D. Li, Y.-P. Gong, H. Li and D. Wu, Abnormal phase transition in $BiNbO_4$ powders prepared by a citrate method, *J. Alloys Compd.*, 2011, **509**, 10230–10233.
18 D. Zhou, H. Wang, X. Yao, X. Wei, F. Xiang and L. Pang, Phase transformation in $BiNbO_4$ ceramics, *Appl. Phys. Lett.*, 2007, **90**, 172910.
19 H. Zhai, B. Chen, H. Luo, H. Li, L. Zheng, J. Yang, H. Liu and Z. Liu, The stability and dielectric performance of $BiNbO_4$ prepared by citrate method assisting sintering process, *Phys. Status Solidi A*, 2016, **213**, 2525–2530.
20 S. Devesa, M. P. Fernandes Graca, F. Henry and L. Cadillon, Costa, Structural, morphological and microwave dielectric properties of (Bi_{1-}*x*Eu*x*)NbO4 ceramics prepared by the sol–gel method, *Int. J. Mater. Eng. Innovation*, 2017, **8**, 12–26.
21 N. A. Zhuk, V. A. Belyy, V. P. Lutoev, B. A. Makeev, S. V. Nekipelov, M. V. Yermolina and L. S. Feltsinger, Mn doped $BiNbO_4$ ceramics: Thermal stability, phase transitions, magnetic properties, NEXAFS and ESR spectroscopy, *J. Alloys Compd.*, 2019, **778**, 418–426.
22 N. A. Zhuk, S. M. Shugurov, M. G. Krzhizhanovskaya, V. A. Belyy, N. A. Sekushin, B. A. Makeev, S. V. Nekipelov, D. S. Beznosikov and Y. A. Busargina, The effect of CuO on the microstructure, spectral characteristics, thermal and electrical properties of BiNbO4 ceramics, *J. Alloys Compd*, 2020, **822**, 153619.
23 N. A. Zhuk, J. A. Busargina, V. A. Belyy, B. A. Makeev, D. S. Beznosikov and M. G. Krzhizhanovskaya, Phase transformations and thermal stability of Ni-doped $BiNbO_4$ ceramics, *Thermochim. Acta*, 2019, **673**, 12–16.
24 W. Jo, J. B. Ollagnier, J. L. Park, E. M. Anton, O. J. Kwon, C. Park, H. H. Seo, J. S. Lee, E. Erdem, R. A. Eichel and J. Roedel, CuO as a sintering additive for (Bi1/2Na1/2)TiO3-BaTiO3-(K0.5Na0.5)NbO3 lead-free piezoceramics, *J. Eur. Ceram. Soc.*, 2011, **31**, 2107–2117.
25 M. Bakiro, S. Hussein Ahmed and A. Alzamly, Effect of pH, Surfactant, and Temperature on Mixed-Phase Structure and Band Gap Properties of BiNbO4 Nanoparticles Prepared Using Different Routes, *Chem.*, 2019, **1**, 89–110.
26 Y. J. Liu, J. W. Zhang, D. W. He, C. Xu, Q. W. Hu, L. Qi and A. K. Liang, Exploring the compression behavior of HP-$BiNbO_4$ under high pressure, *Chin. Phys. B*, 2017, **26**, 116202.
27 Y. Liu, C. Xu, D. He, J. Zhang, Q. Hu and L. Qi, Exploring the phase transition of $BiNbO_4$: A high pressure x-ray diffraction study, *Solid State Commun.*, 2017, **265**, 15–18.
28 H. K. Mao, J. Xu and P. M. Bell, Calibration of the Ruby Pressure Gauge to 800 kbar under quasi-hydrostatic conditions, *J. Geophys. Res.*, 1986, **91**, 4673–4676.
29 S. Klotz, J. C. Chervin, P. Munsch and G. Le, Marchand, Hydrostatic limits of 11 pressure transmitting media, *J. Phys. D*, 2009, **42**, 075413.
30 C. Prescher and V. B. Prakapenka, DIOPTAS: a program for reduction of two-dimensional X-ray diffraction data and data exploration, *High Pressure Res.*, 2015, **35**, 223–230.
31 G. Kresse and J. Furthmuller, Efficient iterative schemes for ab initio total-energy calculations using a plane-wave basis set, *Phys. Rev. B*, 1996, **54**, 11169–11186.
32 J. P. Perdew, K. Burke and M. Ernzerhof, Gradient Approximation Made Simple, *Phys. Rev. Lett.*, 1996, **77**, 3865–3868.
33 S. Devesa, M. P. Graca and L. C. Costa, Structural, morphological and dielectric properties of $BiNbO_4$ ceramics prepared by the sol-gel method, *Mater. Res. Bull.*, 2016, **78**, 128–133.
34 A. J. M. Sales, D. G. Sousa, H. O. Rodrigues, M. M. Costa, A. S. B. Sombra, F. N. A. Freire, M. J. Soares, M. P. F. Graca and J. Suresh Kumar, Power dependent upconversion in Er^{3+}/Yb^{3+} co-doped $BiNbO_4$ phosphors, *Ceram. Int.*, 2016, **42**, 6899–6905.
35 Multani Ayyub and Vijayaraghavan Palkar, Vibrational spectroscopic study of ferroelectric $SbNbO_4$, antiferroelectric $BiNbO_4$, and their solid solutions, *Phys. Rev. B: Condens. Matter Mater. Phys.*, 1986, **34**, 8137–8140.
36 D. Errandonea, Y. Meng, M. Somayazulu and D. Hausermann, Pressure-induced α - > γ transition in titanium metal: a systematic study of the effects of uniaxial stress, *Phys. Rev. B: Condens. Matter Mater. Phys.*, 2005, **355**, 116–125.
37 R. B. Luo, W. Zeng, Y. D. Wu, W. L. Jiang, B. Tang, M. Zhong and Q. J. Liu, First-principles calculations on electronic, optical and photocatalytic properties of $BiNbO_4$, *Mater. Sci. Semicond. Process.*, 2022, **140**, 106391.
38 X. Cheng, J. Guan, L. Jiang, H. Zhang, P. Wang, A. O. Adeniyi, Y. Yao, L. Su and Y. Song, Pressure-induced structural transformations and new polymorphs in $BiVO_4$, *Phys. Chem. Chem. Phys.*, 2020, **22**, 10238–10246.
39 X. Dong, Z. Huangfu, Y. Liang, C. Yuan, S. Li, X. Zhu, L. Jiang, K. Yang, Y. Wang, X. Cheng, L. Su and G. Yang, Increasing Doping Solubility of RE^{3+} Ions in Fergusonite $BiVO_4$ via Pressure-Induced Phase Transition, *J. Phys. Chem. C*, 2021, **125**, 22388–22395.
40 X. Cheng, Y. Ren, J. Shang and Y. Song, Contrasting Structural Stabilities and New Pressure-Induced Polymorphic Transitions of Scheelite- and Zircon-Type $ZrGeO_4$, *J. Phys. Chem. C*, 2017, **121**, 723–730.
41 X. Cheng, D. Guo, S. Feng, K. Yang, Y. Wang, Y. Ren and Y. Song, Structure and stability of monazite- and zircon-type $LaVO_4$ under hydrostatic pressure, *Opt. Mater.*, 2015, **49**, 32–38.

